JOURNAL OF CHEMICAL & ENGINEERING DATA

ARTICLE

pubs.acs.org/jced

Physiochemical Properties of γ-Al_2O_3−MgO and γ-Al_2O_3−CeO_2 Composite Oxides

Muhammad Farooq,[†] Anita Ramli,[*,†] and Duvvuri Subbarao[‡]

[†]Department of Chemical Engineering, Universiti Teknologi PETRONAS Bandar Seri Iskandar, 31750 Tronoh, Perak, Malaysia

[‡]Fundamental and Applied Sciences Department, Universiti Teknologi PETRONAS Bandar Seri Iskandar, 31750 Tronoh, Perak, Malaysia

ABSTRACT: A series of γ-Al_2O_3−MgO and γ-Al_2O_3−CeO_2 composite oxides with different respective MgO and CeO_2 loadings were prepared successfully via wet impregnation method. The synthesized composite oxides were characterized by X-ray diffraction (XRD), field emission scanning electron microscopy−energy dispersive X-ray analysis (FESEM-EDAX), thermogravimeric analysis (TGA), X-ray photoelectron spectroscopy (XPS), X-ray fluorescence (XRF) and Brunauer−Emmett−Teller (BET) methods. The point of zero charge (PZC) of oxides/mixed oxides was determined by salt addition and potentiometric methods to explore the effects of MgO and CeO_2 contents on the PZC of γ-Al_2O_3. The results showed that, as the MgO loading was increased, PZC of alumina also increased linearly. However, in the case of CeO_2 addition, the change in PZC of γ-Al_2O_3 was not so significant. Moreover, the PZC of these synthesized composite oxides varied between the PZCs of pure oxides of Al_2O_3, MgO, and CeO_2. Further, it was noted that, at lower MgO and CeO_2 loadings, the structure of γ-Al_2O_3 was protected; however, at higher loadings, a change in the structure of γ-Al_2O_3 was observed. XPS results showed that binding energies decreased as MgO and CeO_2 loadings were increased. This decrease in the binding energies of Mg and Ce was attributed to the change in their chemical environment which caused change in the average valence state (oxidation state) of elements.

1. INTRODUCTION

Transition metal oxides offer a wide range of properties which provide the foundation for a broad range of potential applications in various fields.[1] Mixed metal oxides are chemical compounds which are formed by the chemical combinations of two or more metal oxides. Transitions mixed metal oxides exhibit different chemical and textural properties as compared to the single oxide systems which give them an advantage for use in a wide variety of technologically important catalytic processes.[2,3] In addition to catalytic applications, these mixed oxides have also been employed for various other purposes such as photoconductive thin films, gas sensors, and in fuel cell and ceramic technologies.[4−7] It is established in the literature that mixing two dissimilar oxides adds another parameter since they are liable to form new stable compounds, which can lead to totally different physicochemical properties and catalytic behaviors. Mixed oxides possess high surface area, profound surface acid−base properties, high thermal stability, and strong mechanical strength and hence make them potential candidates as effective materials for different applications.[8−10] Mixed metal oxides of γ-Al_2O_3−MgO and γ-Al_2O_3−CeO_2 exhibit a wide range of properties and phenomena. The diverse structures adopted by these mixed metal oxides are helpful to demonstrate the relationship between structures and properties.[11] The properties of γ-Al_2O_3 can be modified by introducing a second suitable metal oxide to form a composite oxide with suitable acid−base properties. Among various metal oxides MgO is considered a promising metal oxide which can modify the properties of alumina in the γ-Al_2O_3−MgO mixed oxides due to the strong basic characteristics of MgO. Moreover, they have a high mechanical resistance and thermal stability due to complex bond formation.[12] Similarly, γ-Al_2O_3−CeO_2 mixed oxides show better textural stability, enhanced redox activity, which is attributed to higher oxygen mobility in the mixed oxide lattice and hence better resistance to the chemical (redox) deactivation upon thermal aging.[13] The improved properties of Al_2O_3−CeO_2 mixed oxides are due to the fluorite type structure of CeO_2 with large vacant octahedral holes, facilitating the oxygen mobility through the defect structure.

The surface science of mixed metal oxides has received great attention in this modern age of industrialization to explore their applications in various areas. The textural and surface properties of the mixed oxides as well as their activity can be controlled by the selection of an appropriate chemical combination and preparation method.[14] An oxide surface contains terminal hydroxyl groups that protonate or deprotonate depending on the acidity of the solution. The pH at which the hydroxyl groups are neutral is termed as point of zero charge (PZC). Below this pH, the hydroxyl groups protonate and become positively charged; hence the surface absorbs anionic metal complexes. Above the PZC, the hydroxyl groups deprotonate, become negatively charged, and thus adsorb cations.[15] This can easily be demonstrated by a model as shown in the Figure 1. The corresponding reactions are given as:

$$M{-}OH + H^+ \leftrightarrow M{-}OH^{+2} \qquad pH < PZC \qquad (1)$$

$$M{-}OH \leftrightarrow M{-}O^- + H^+ \qquad pH > PZC \qquad (2)$$

Several attempts have been made to explore the surface properties of mixed oxides for a wide range of applications. Waseem et al.[16]

Received: June 17, 2011
Accepted: October 31, 2011
Published: December 05, 2011

dx.doi.org/10.1021/je200597h | *J. Chem. Eng. Data* 2012, 57, 26–32

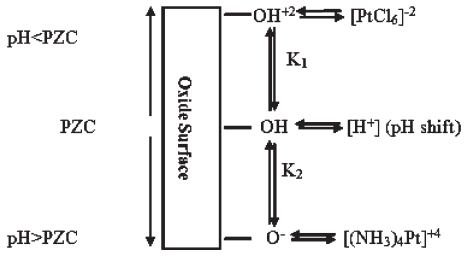

Figure 1. Point zero charge model.

investigated the surface charge properties of mixed oxides of iron and silicon by salt addition and zeta potential methods. The authors concluded that PZC was controlled by the silica contents in the mixed oxide systems. Mattijevic et al.[17] carried out a detailed study of silica−alumina mixed oxides. Their results showed that the PZC of mixed oxide systems varied between the PZCs of their constituent pure oxides. Anderson and Benjamin[18] pointed out that the surface properties of iron hydroxides prepared in the presence of silica depend on the Si content, and increasing the Si:Fe molar ratio decreases the PZC of the solid. Similarly Subraminian et al.[19] investigated the surface charge properties of alumina and titania mixed oxide systems and concluded that the PZCs of these mixed oxides showed variation between the PZCs values for the two pure phases.

The present work deals with the preparation of mixed oxides such as γ-Al_2O_3−MgO and γ-Al_2O_3−CeO_2 containing different loadings of MgO and CeO_2 (5, 10, 15, and 20 wt % with respect to Al_2O_3), respectively, and characterization with various techniques to explore the effects of MgO and CeO_2 contents on the surface properties of alumina in the composite oxides. Furthermore, the physiochemical properties of synthesized mixed oxides are correlated with respect to MgO and CeO_2 loadings in their composite oxides.

2. EXPERIMENTAL SECTION

2.1. Preparation of Mixed Oxides. γ-Al_2O_3−MgO and γ-Al_2O_3−CeO_2 mixed oxides containing different loadings of MgO and CeO_2 (5, 10, 15, 20 wt % with respect to Al_2O_3) respectively were prepared by wet impregnation method.[20] In this method, the required amount of magnesium nitrate hexahydrate $Mg(NO_3)_2 \cdot 6H_2O$ (Merck, 99.99 %) was dissolved in distilled water to obtain the required loading of MgO in Al_2O_3−MgO mixed oxides. A required amount of precalcined γ-Al_2O_3 (Merck, 190 $m^2 \cdot g^{-1}$) was then added slowly into the solution, slightly in excess with respect to the pore volume of the γ-Al_2O_3, with constant stirring to avoid the formation of a thick paste. This mixture was stirred for 3 h at room temperature, and then water was slowly evaporated from the paste by heating gently at 70 °C. The solid samples were dried at 110 °C for 12 h in an oven and calcined at 500 °C in the presence of air in muffle furnace for 5 h to get γ-Al_2O_3−MgO mixed oxides with different MgO loadings. Similarly, Al_2O_3−CeO_2 mixed oxides were prepared by impregnating γ-Al_2O_3 with slightly excess aqueous solution of Ce $(NO_3)_3 \cdot 6H_2O$ (Sigma Aldrich, 99.9 %) to obtain the required loading of CeO_2 contents. The mixture was dried in oven at 110 °C for 12 h and then calcined at 500 °C in a muffle furnace for 5 h.

2.2. Characterization. The N_2 physisorption was carried out in order to evaluate the textural properties such as the specific surface area (S_{BET}), mean pore diameter (D_p), and total pore volume (V_t) of the synthesized oxides/mixed oxides with different MgO and CeO_2 loading. The nitrogen adsorption and desorption isotherms were measured at −196 °C on an ASAP 2020 system in static measurement mode. The samples were degassed at 160 °C for 4 h before the measurement. S_{BET} was obtained by the multipoint Brunnuer−Emmet-Teller method (BET) and mean pore diameter by the Barret−Joyner−Halenda method (BJH) from the desorption isotherm. The morphology and elemental composition of oxides/mixed oxides were studied by field emission scanning electron microscopy (JEOL 6340). X-ray diffraction (XRD) of samples was performed on a JEOL X-ray diffractometer, model JDX-3530 M with Mn filtered Cu Kα radiations.

Thermogravimetry and derivatives of thermogravimetry (TG-DTG) were performed by a Perkin-Elmer Pyris 1 from room temperature to 700 °C at a heating rate of 10 $°C \cdot min^{-1}$ and nitrogen gas flow of 20 $mL \cdot min^{-1}$.

X-ray photoelectron spectroscopy (XPS), using Shimadzu equipment with a Mg Kα X-ray radiation source (E = 1253.6 eV), was used to analyze the surface composition of the metal oxides. The line C1s with a binding energy of 284.6 eV was used as the reference. Similarly, the atomic concentration ratios in the outer layers of the samples were determined from the corresponding XPS area ratios by using the effective ionization cross section of the ejected electrons.

Elemental analysis was carried out on the Bruker S4 PIONEER X-ray fluorescence spectrum (XRF) using an Ru target and 4 kW maximum power.

2.3. PZC Determination. *2.3.1. Salt Addition Method.* The PZCs of all samples were determined by using the salt addition method.[21] In this method 0.01 M $NaNO_3$ solution was prepared in preboiled deionized water to eliminate CO_2. A portion of 40 mL of 0.01 M $NaNO_3$ solutions was taken in different titration flasks. The pH values of these solutions were adjusted to 2, 3, 4, 5, 6, 7, 8, 9, 10, 11, and 12 using 0.01 M HNO_3 and 0.01 M NaOH solutions. The initial pH values were recorded with pH meter model BOECO BT-600 (Germany) with a temperature probe and pH electrode of research grade. About 0.2 g of given sample was then added to each flask and was shaken for 48 h in a shaker bath at 25 °C. After 48 h, the final pH values were recorded and then ΔpH (difference between initial and final pH) values were plotted against initial pH values. The PZC values were calculated from ΔpH verses $pH_{initial}$ plots, which is the pH at which ΔpH is zero, that is, $pH_{initial} = pH_{final}$.

2.3.2. Fast Titration (Potentiometric Titration) Method. The PZCs of synthesized samples were also determined by the potentiometric titration method.[22] Potentiometric titrations for various oxides/mixed oxides were conducted in a thermostatted double walled Pyrex cell of 100 mL capacity, maintained at constant temperature using thermostatted water bath via a circulating pump and using a magnetic stirrer with Teflon coated stirring bars. A portion of 30 mL of 0.01 M $NaNO_3$ solution containing 0.2 g of sample was equilibrated for 40 min with continuous magnetic stirring at room temperature. A sample of 2 mL of 0.01 M HNO_3 was then added, and the suspension was agitated further for 20 min. The new pH value of the suspension was recorded as the initial pH with pH meter model BOECO BT-600 (Germany) with a temperature probe and pH electrode of research grade. The suspension was then titrated with 0.01 M NaOH by the addition of 0.2 mL from a microburet of a very fine tip. Following each addition of the titrant (0.01 M NaOH), the

dx.doi.org/10.1021/je200597h |J. Chem. Eng. Data 2012, 57, 26–32

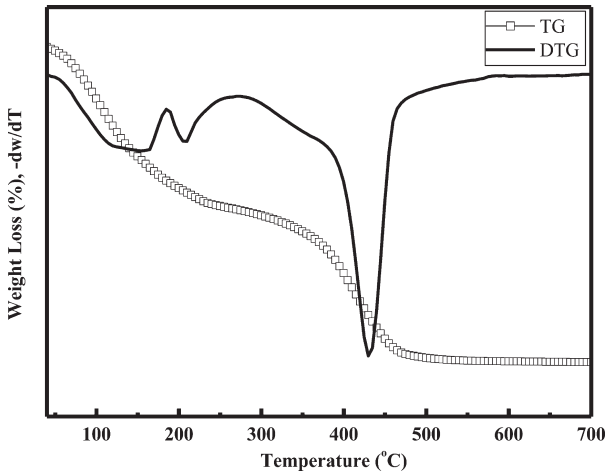

Figure 2. TG and DTG curves for sample loaded with $Mg(NO_3)_2 \cdot 6H_2O$ to prepare Al_2O_3—20 wt % MgO mixed oxide.

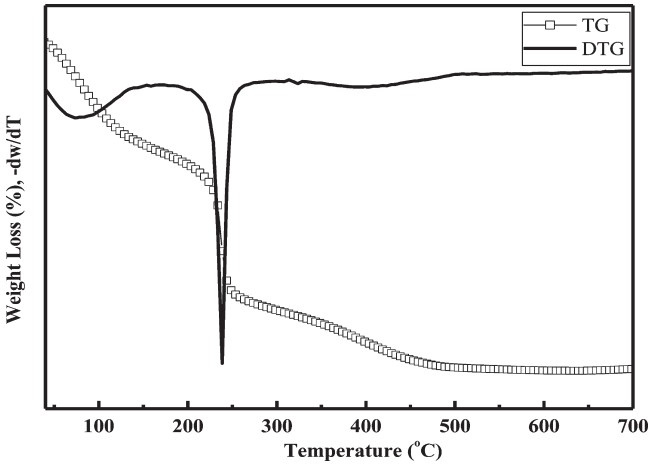

Figure 3. TG and DTG curves for sample loaded with $Ce(NO_3)_2 \cdot 6H_2O$ to prepare Al_2O_3—20 wt % CeO_2 mixed oxide.

pH of the suspension was recorded after every 2 min. The surface charge density σ_o ($\mu C \cdot m^{-2}$) was calculated using the formula:

$$\sigma_o = \frac{[C_A - C_B + [OH^-] - [H^+]]F}{mS} \quad (3)$$

where C_A ($mol \cdot dm^{-3}$) and C_B ($mol \cdot dm^{-3}$) are the concentrations of acid and base added to the suspension, $[OH^-]$ and $[H^+]$ are the concentrations of OH^- and H^+ ions as measured from the pH of the suspension, F ($C \cdot mol^{-1}$) is the Faraday constant, m is the mass of oxides/mixed oxides (g), and S ($m^2 \cdot g^{-1}$) is the specific surface area of the given sample.

3. RESULTS AND DISCUSSION

Figures 2 and 3 show the representative thermogravimetry and derivatives of thermogravimetry (TG-DTG) for samples loaded with $Mg(NO_3)_2 \cdot 6H_2O$ and $Ce(NO_3)_2 \cdot 6H_2O$ to synthesize mixed oxides of γ-Al_2O_3—MgO and γ-Al_2O_3—CeO_2 containing 20 wt % MgO and CeO_2 contents, respectively. The TG-DTG curves for sample loaded with Mg $(NO_3)_2 \cdot 6H_2O$ showed three endothermic peaks at (135, 208, and 430) °C which are attributed to the evaporation of absorbed water, removal of water of crystallization, and decomposition of nitrate molecules, respectively. Along with the loss of water of crystallization, some nitrate anions undergo partial decomposition.[23,24] However, the decomposition of nitrate molecules was completed at about 500 °C, and above 600 °C there is no significant weight loss. Similarly, TG-DTG curves for sample loaded with $Ce(NO_3)_2 \cdot 6H_2O$ exhibited two endothermic peaks at about (73 and 239) °C. The endothermic peak at 73 °C is assigned to evaporation of absorbed water in the sample, where the endothermic peak at 239 °C is attributed to the removal of water of crystallization and decomposition of nitrate molecules in the sample.[25] In addition, there appeared a small endothermic peak at 409 °C, which may be attributed to the decomposition of remaining nitrate molecules in the sample. The curve further shows that there is no significant weight loss above 550 °C, which means that the decomposition of $Ce(NO_3)_2 \cdot 6H_2O$ has finished.

Table 1. Effect of MgO Loading on the Textural Properties: Specific Surface Area (S_{BET}), Pore Volume (V_p), and Mean Pore Diameter (D_p)

MgO content (wt %)	0	5	10	15	20
SA ($m^2 \cdot g^{-1}$)	186	167	151	142	134
V_p ($cc \cdot g^{-1}$)	0.241	0.179	0.161	0.158	0.142
D_p (Å)	78.43	72.401	67.31	59.63	49.36

Table 2. Effect of CeO_2 Loading on the Textural Properties: Specific Surface Area (S_{BET}), Pore Volume (V_p), and Mean Pore Diameter (D_p)

CeO_2 content (wt %)	0	5	10	15	20
SA ($m^2 \cdot g^{-1}$)	186	171	155	146	140
V_p ($cc \cdot g^{-1}$)	0.241	0.187	0.174	0.160	0.148
D_p (Å)	78.43	77.52	61.01	58.59	51.46

The specific surface area (S_{BET}), total pore volume (V_p), and mean pore diameter (D_p) of γ-Al_2O_3—MgO mixed oxide samples loaded with different MgO contents are given in Table 1. It can be seen from the results that the addition of magnesia contents caused a decrease in the surface area, pore volume, and mean pore diameter. The same trend was also observed for Al_2O_3—CeO_2 mixed oxides as the CeO_2 loading was increased (Table 2). This decrease in S_{BET}, V_p, and D_p is due to the fact that the addition of MgO and CeO_2 blocked some of the pores of alumina by plunging into the pores during the preparation and formation of some complex oxides on the surface as a result of oxide reaction during calcination in the furnace.

Figures 4 and 5 illustrate the XRD patterns for mixed oxides of γ-Al_2O_3—MgO and γ-Al_2O_3—CeO_2 with different MgO and CeO_2 contents, respectively. The XRD profiles shown in the Figure 4 exhibited characteristic peaks of γ-Al_2O_3 and MgO at 66.8, 45.55, and 37.3 and 62.15 and 42.7, respectively. However, no characteristic peaks corresponding to $Mg(NO_3)_2 \cdot 6H_2O$ were observed, showing that all of the nitrate molecules were completely decomposed at calcination temperature (500 °C). Further it can be seen from the XRD patterns that samples loaded with 5 and 10 wt % MgO contents did not exhibit characteristic peaks of crystalline MgO, showing good dispersion of MgO with monolayer or submonolayer formation on the surface of γ-Al_2O_3. However, above these contents, as the MgO loading was increased, the XRD profiles changed with the appearance of

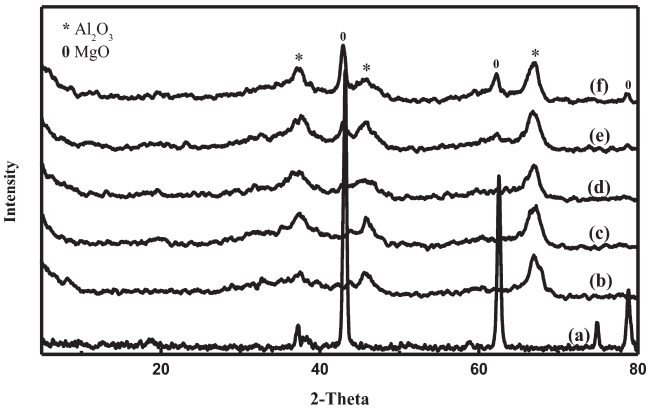

Figure 4. XRD pattern for (a) MgO, (b) γ-Al_2O_3, (c) Al_2O_3−5 wt % MgO, (d) Al_2O_3−10 wt % MgO, (e) Al_2O_3−15 wt % MgO, (f) Al_2O_3−20 wt % MgO.

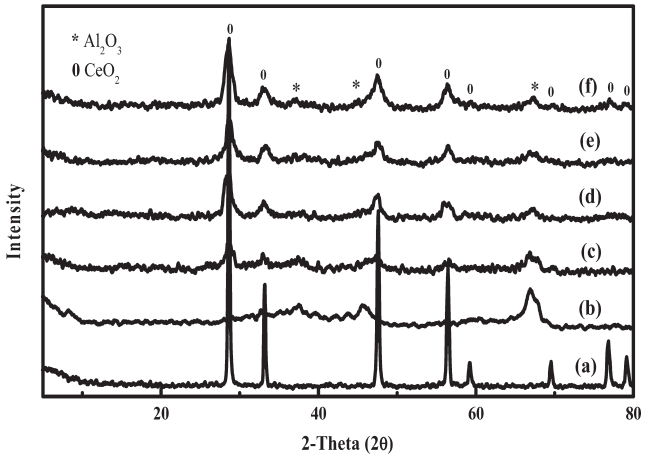

Figure 5. XRD pattern for (a) CeO_2, (b) γ-Al_2O_3, (c) Al_2O_3−5 wt % CeO_2, (d) Al_2O_3−10 wt % CeO_2, (e) γ-Al_2O_3−15 wt % CeO_2, (f) Al_2O_3−20 wt % CeO_2.

new peaks at 66.8, 45.55, and 37.3 and 62.15 and 42.7 corresponding to crystalline MgO on the surface of γ-Al_2O_3. This showed that the addition of MgO at lower scale did not affect the structure of alumina; however, high loading of MgO affected the structure of γ-Al_2O_3 which is in agreement with the results reported by other authors.[26,27] Similarly, Figure 5 displays XRD patterns for Al_2O_3−CeO_2 mixed oxides with varying amounts of CeO_2. The characteristic peaks observed at 28.76, 33.22, 47.67, 56.46, 59.29, 69.56, 76.86, and 79.25 are corresponding to CeO_2 in the samples with different CeO_2 contents. It is clear from the XRD patterns that as the CeO_2 loading increased the intensity of peaks corresponding to CeO_2 also increased showing an increase in crystallinity, where the peak intensities corresponding to γ-Al_2O_3 decreased. Thus XRD results confirmed the monolayer or submonolayer formation at lower loadings of MgO and CeO_2, whereas formation of crystalline MgO and CeO_2 with high contents of these oxides on the surface of γ-Al_2O_3 was reported in the literature.[28]

The surface morphology and elemental composition of γ-Al_2O_3−MgO and γ-Al_2O_3−CeO_2 mixed oxides were studied by emission scanning electron microscopy (FESEM) and energy

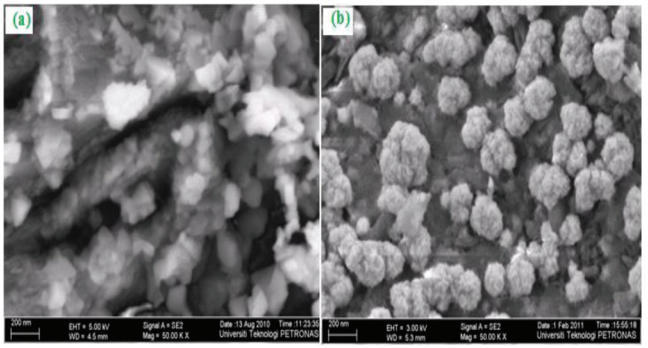

Figure 6. Representative FESEM images of mixed oxides. (a) γ-Al_2O_3−20 wt % MgO, (b) γ-Al_2O_3−20 wt % CeO_2.

Table 3. Mg/Al Ratio in Al_2O_3−MgO Mixed Oxides Determined by EDAX, XRF, and Theoretically

	Mg/Al atomic ratio in the mixed oxides with different MgO loadings		
MgO content wt %	EDAX	theoretical values	XRF
5	0.0493	0.0600	0.059
10	0.1152	0.1265	0.127
15	0.1954	0.2010	0.213
20	0.2301	0.2846	0.279

Table 4. Ce/Al Ratio in Al_2O_3−CeO_2 Mixed Oxides Determined by EDAX, XRF, and Theoretically

	Ce/Al atomic ratio in the mixed oxides with different CeO_2 loadings		
CeO_2 content wt %	EDAX	theoretical values	XRF
5	0.0513	0.0600	0.059
10	0.1602	0.1265	0.127
15	0.2154	0.2010	0.213
20	0.2621	0.2846	0.265

dispersive X-ray analysis (EDAX). However, only representative photographs are shown in the Figure 6a and b. It is clear from Figure 6a that the Al_2O_3−MgO sample did not possess a definite shape and that the morphology slightly changed as the MgO loading was increased with the appearance of crystalline MgO on the surface of alumina. However, in the case of γ-Al_2O_3−CeO_2 mixed oxide sample uniformly distributed, spherical shaped particles were found with little agglomeration on the surface of γ-Al_2O_3 as shown in Figure 6b. The dimension of the particles was found to be within the range of (5 to 10) μm. The micrograph further showed the polycrystalline particle formation on the surface. These polycrystalline spherical structures are formed from primary crystallites which fused together to make large-sized spheres with polycrystalline substructures.[29] The homogeneous distribution of MgO and CeO_2 over the surface of alumina was further conformed by EDAX. The elemental composition determined by EDAX is given in Tables 3 and 4. Further, the EDAX results showed close agreement with values determined by XRF

dx.doi.org/10.1021/je200597h |J. Chem. Eng. Data 2012, 57, 26–32

Table 5. Variation of Binding Energies and Mg/Al Ratios with MgO Content in Mixed Oxides

	binding energy		atomic ratio
MgO contents (wt %)	Al2p	Mg2p	Mg/Al
5	74.73	50.74	0.198
10	74.54	50.60	0.239
15	74.35	50.45	0.402
20	74.29	50.30	0.523

Table 6. Variation of Binding Energies and Ce/Al Ratios with CeO_2 Contents in Mixed Oxides

	binding energy		atomic ratio
CeO_2 contents (wt %)	Al2p	Ce3d	Ce/Al
5	74.80	883.51	0.210
10	74.64	883.40	0.242
15	74.48	883.23	0.411
20	74.32	883.05	0.509

and theoretical values, showing that synthesized composite oxides contained as much MgO and CeO_2 contents in their respective mixed oxides as were loaded during impregnation.

XPS analysis results for Al_2O_3-MgO and $Al_2O_3-CeO_2$ mixed oxides are given in Tables 5 and 6, respectively. It can be seen from the results that binding energies of Al2p, Mg2p, and Ce3d slightly decreased as the MgO and CeO_2 loadings were increased. The difference in the binding energies is attributed to the change in the coordination number of Mg and Ce atoms, which may be due to an interaction of MgO and CeO_2 with alumina, respectively.[30] The stronger the interaction between the components, the greater the binding energies will be. The binding energies of Al2p, Mg2p, and Ce3d depend on the chemical environment of Al, Mg, and Ce atoms. When MgO and CeO_2 contents were low, these oxides dispersed as monolayer or submonolayer on the surface of alumina causing stronger interaction and, hence, higher binding energies. However, at higher loadings these oxides form crystalline particles which show comparatively weak interactions and hence lower binding energies. It has been reported that the coordination structures of Mg−O shells within MgO are not affected by the dispersion of MgO on the surface of γ-Al_2O_3; however, Mg−Mg networks change effectively.[31] Moreover, the increase in binding energies with lower loadings of MgO and CeO_2 was due to stronger interaction between γ-Al_2O_3/MgO and γ-Al_2O_3/CeO_2 in the composite oxides as Mg^{2+}/Ce^{3+} cations occupied the surface vacant sites of alumina with monolayer formation, generating a new structure of Mg−O−Al. Therefore, the binding energies of Mg2p and Ce3d of dispersed phases of MgO and CeO_2 are quite different from that of their crystalline species.[32,33] Similarly, the Mg/Al and Ce/Al ratios determined by XPS were higher than those reported by EDAX, XRF, and theoretical values. XPS is a surface chemical analysis technique that can be used to analyze the surface chemistry of a material and contains the characteristics of a surface layer. Therefore, the Mg/Al and Ce/Al ratios given by the XPS indicated the Mg and Ce enrichment with spontaneous dispersion to form a monolayer on the surface of

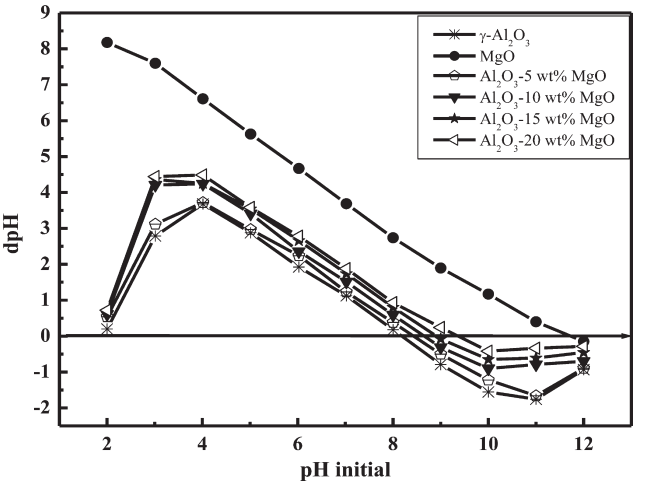

Figure 7. Plots of ΔpH vs initial pH for oxides/mixed oxides with different MgO contents.

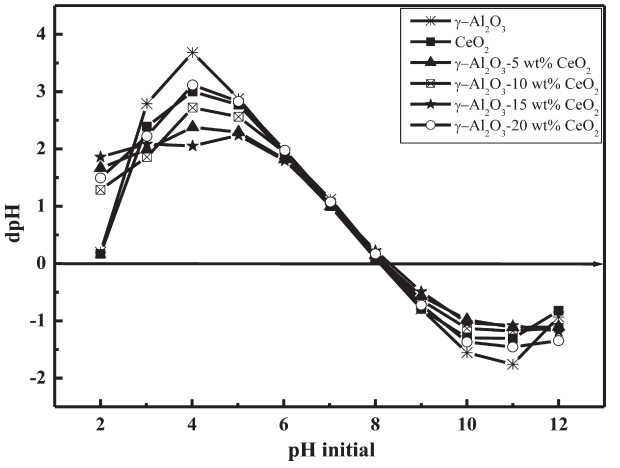

Figure 8. Plots of ΔpH vs initial pH for oxides/mixed oxides with different CeO_2 contents.

γ-Al_2O_3 even with the samples having lower contents of MgO and CeO_2 in their respective mixed oxides.[31]

The PZC of pure commercial γ-Al_2O_3, MgO, CeO_2, and mixed oxides of γ-Al_2O_3-MgO and γ-$Al_2O_3-CeO_2$ containing different MgO and CeO_2 contents, respectively, was determined as shown in Figures 7 and 8. The result showed that the addition of MgO to γ-Al_2O_3 caused a change in the pH values. When ΔpH was plotted against initial pH values, PZC was obtained for different samples having different percentages of MgO. The PZC is the pH where the net surface charge of an oxide is zero; therefore, ΔpH is zero. The PZC for γ-Al_2O_3 was found to be 8.2, and that for pure commercial MgO was 11.6. However, the PZC values for mixed oxides with different loadings of MgO were found to vary between the PZCs of pure oxides of γ-Al_2O_3 and magnesia as reported elsewhere[34,35] (Table 7). Also from the results it was noted that the addition of MgO to alumina caused a gradual increase in the surface charge of these mixed oxides. MgO exhibits basic behavior in the aqueous solution with a PZC of 11.6. As the MgO content increased the MgO surface charge became predominant. The PZCs of mixed oxides moved towards the PZC of MgO. Similarly, the PZC values for CeO_2

Table 7. Variation of PZC of Al_2O_3 with Respect to MgO Contents

compound	MgO contents (wt %)	PZC
γ-Al_2O_3	0	8.2
Al_2O_3−MgO	5	8.4
Al_2O_3−MgO	10	8.7
Al_2O_3−MgO	15	8.9
Al_2O_3−MgO	20	9.3
MgO	99.98	11.6

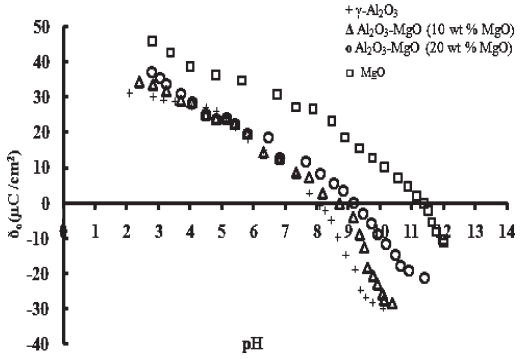

Figure 9. Variation of surface charge density δ_o of oxides/mixed oxides with different MgO loadings vs pH at room temperature.

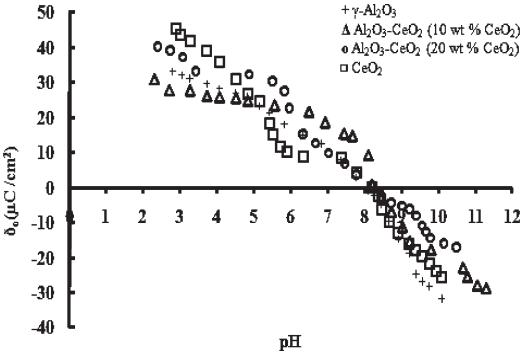

Figure 10. Variation of surface charge density δ_o of oxides/mixed oxides with different CeO_2 loading vs pH at room temperature.

and γ-Al_2O_3−CeO_2 mixed oxides with different CeO_2 contents were found to be 8.1 and 8.1 ± 0.2, respectively. Further, it was noted that PZC values for CeO_2 and Al_2O_3−CeO_2 were close to that of pure γ-Al_2O_3. This showed that at lower loadings of MgO alumina sustains its properties; however, at higher loadings of MgO the solid showed basic properties due to high contents of MgO in the mixed oxide samples. But in the case of CeO_2, due to its poor basic behavior, the PZC of γ-Al_2O_3 did not change, and the surface charge of γ-Al_2O_3 remained close to the PZC value of γ-Al_2O_3.

Similarly Figures 9 and 10 show the variation of surface charge density δ_o vs pH values for oxide/mixed oxide samples containing different MgO and CeO_2 contents. It can be seen from Figures 9 and 10 that the surface charge densities at room temperature cross the pH line at the points corresponding to the PZCs of the oxide systems. The PZC values for MgO, γ-Al_2O_3, and Al_2O_3−MgO mixed oxides with 10 and 20 wt % MgO loading were found to be 11.4, 8.2, 8.7, and 9.2, respectively. In the same way, the PZC values for CeO_2 and Al_2O_3−CeO_2 mixed oxides with 10 and 20 wt % CeO_2 loading were recorded as 8.1, 8.2, and 8.19, respectively. The PZC values determined for various oxides/mixed oxides from the titration curves have close agreement with the values calculated by the salt addition method.

4. CONCLUSION

γ-Al_2O_3−MgO and γ-Al_2O_3−CeO_2 mixed oxides with varying amounts of MgO and CeO_2 were successfully prepared by the wet impregnation method. The PZC of oxides/mixed oxides was determined by conventional salt addition and fast potentiometric titration methods. The results obtained from both methods showed that the PZC of mixed oxides varied between the PZCs of their constituent pure oxides. The surface area of mixed oxides decreased slightly due to plunging of MgO and CeO_2 molecules into γ-Al_2O_3 pores. XRD results showed that lower loadings of MgO and CeO_2 did not cause change in the phase and structure of alumina; however, when the loading of MgO and CeO_2 was increased, change was observed in the phase and structure of alumina with appearance of crystalline MgO and CeO_2 in their composite oxides. The Mg/Al and Ce/Al ratios determined by XPS were higher than the ratios determined by XRF and theoretical values. This trend showed the enrichment of the surface with Mg and Ce with monolayer or submonolayer formation, as XPS gives the surface analysis. Moreover, the XPS results showed that binding energies decreased as the MgO and CeO_2 contents increased in the corresponding mixed oxides. This is probably due to the change in the chemical environment of Mg and Ce atoms which caused a change in the coordination number and hence in the binding energies.

AUTHOR INFORMATION

Corresponding Author

*E-mail address: anita_ramli@petronas.com.my

Funding Sources

This work is supported by Universiti Teknologi PETRONAS Malaysia. The authors are grateful for the Graduate Assistantship Scheme provided for M.F.

REFERENCES

(1) Cao, J.; Wu, J. Strain effects in low-dimensional transition metal oxides. *Mater. Sci. Eng. Res.* **2011**, *71*, 35–52.

(2) Kung, H. H. *Transition Metal Oxides: Surface Chemistry and Catalysis*, 1st ed.; Elsevier Science Publishers: New York, 1989.

(3) Henrich, V. E.; Cox, P. A. *The Surface Science of Metal Oxides*; Cambridge University Press: Cambridge, U.K., 1994.

(4) Zakrzewska, K. Mixed oxides as gas sensors. *Thin Solid Films* **2001**, *391*, 229–238.

(5) Joskowska, D.; Pomoni, K.; Vomvas, A.; Koscielska, B.; Anastassopoulos, D. L. On electrical and photoconductive properties of mixed Nb_2O_5/TiO_2 sol−gel thin films. *J. Non-Cryst. Solids* **2010**, *356*, 2042–2048.

(6) Zhi, K.; Liu, Q.; Zhao, R.; He, R.; Zhang, L. Preparation and characterization of Cu-Ce-La mixed oxides as water-gas shift catalyst for fuel cell applications. *J. Rare Earths* **2008**, *26*, 538–543.

(7) Sathiyamoorthy, D.; Ghanwat, S. J.; Tripathi, B. M.; Danani, C. Novel mixed oxide ceramics for neutron multiplication and tritium generation. *J. Nucl. Mater.* **2011**, DOI: 10.1016/j.jnucmat.2010.12.138.

(8) Reddy, B. M.; Khan, A. Recent Advances on TiO_2-ZrO_2 Mixed Oxides as Catalysts and Catalyst Supports. *Catal. Rev.* **2005**, *47*, 257–296.

(9) Kumar, M.; Aberuagba, F.; Gupta, J. K.; Rawat, K. S.; Sharma, L. D.; Murali Dhar, G. Temperature-programmed reduction and acidic properties of molybdenum supported on $MgO-Al_2O_3$ and their correlation with catalytic activity. *J. Mol. Catal. A: Chem.* **2004**, *213*, 217–223.

(10) Chowdhury, A. N.; Rahim, A.; Ferdosi, Y. J.; Azam, M. S.; Hossain, M. M. Cobalt−nickel mixed oxide surface: A promising adsorbent for the removal of PR dye from water. *Appl. Surf. Sci.* **2010**, *256*, 3718–3724.

(11) Richards, R. *Surface and nanomolecular catalysis*; CRC Press Taylor & Francis Group: Boca Raton, FL, 2006; pp 40−42.

(12) Carvalho, L. S.; Martins, A. R.; Reyes, P.; Oportus, M.; Vicentini, V.; Rangel, M. C. Preparation and characterization of $Ru/MgO-Al_2O_3$ catalysts for methane steam reforming. *Catal. Today* **2009**, *142*, 52–60.

(13) Adachi, G.; Imanaka, N.; Kang, Z. C. *Binary rare earth oxides*, 1st ed.; Kluwer Academic Publishers: Netherlands, 2004.

(14) Buckley, R. W. *Solid state chemistry research trends*, 1st ed.; Nova Science Publisher, Inc.: New York, 2007.

(15) Hao, X.; Quach, L.; Korah, J.; Spieker, W. A.; Regalbuto, J. R. The control of platinum impregnation by PZC alteration of oxides and carbon. *J. Mol. Catal. A: Chem.* **2004**, *219*, 97–107.

(16) Waseem, M.; Mustafa, S.; Naeem, A.; Koper, G. J. M.; Salah-ud-Din Physiochemical properties of mixed oxides of iron and silicon. *J. Non-Cryst. Solids* **2010**, *356*, 2704–2708.

(17) Mattijevic, E.; Mangravvite, F. J., Jr.; Cassell, E. A. Stability of colloidal silica. IV. The silica-alumina system. *J. Colloid Interface Sci.* **1971**, *35*, 560–568.

(18) Anderson, P. R.; Benjamin, M. M. Effect of Silicon on the Crystallization and Adsorption properties of Ferric oxides. *Environ. Sci. Technol.* **1985**, *19*, 1048–1053.

(19) Subraminian, S.; Noh, J. S.; Schwarz, J. A. Determination of the point of zero charge of composite oxides. *J. Catal.* **1988**, *114*, 433–439.

(20) Perego, C.; Villa, P. Catalyst Preparation methods. *Catal. Today* **1997**, *34*, 281–305.

(21) Mustafa, S.; Dilara, B.; Nargis, K.; Naeem, A.; Shahida, P. Surface properties of the mixed oxides of iron and silica. *Colloids Surf., A* **1997**, *205*, 273–282.

(22) Davis, J. A.; James, R. O.; Leckie, J. O. Surface ionization and complexation at the oxide/water interface: I. Computation of electrical double layer properties in simple electrolytes. *J. Colloid Interface Sci.* **1978**, *63*, 480–499.

(23) El-Shobaky, H. G.; Mokhtar, M.; Ahmed, A. S. Effect of MgO-doping on solid-solid interactions in MoO_3/Al_2O_3 system. *Thermochim. Acta* **1999**, *327*, 39–46.

(24) Dou, B.; Chen, H.; Song, Y.; Tan, C. Synthesis and characterization of heterostructured nanohybrid of $MgO-TiO_2-Al_2O_3$/montmorillonite. *Mater. Chem. Phys.* **2011**, *130*, 63–66.

(25) Alves, A. K.; Berutti, F. A.; Clemens, F.; Graule, T.; Bergmann, C. P. The effect of heat treatment on CeO_2 and Y_2O_3 doped CeO_2 electrospun fibers. *Rev. Adv. Mater. Sci.* **2009**, *21*, 200–204.

(26) Koo, K. Y.; Roh, H. S.; Jung, U. H.; Seo, D. J.; Seo, Y. S.; Yoon, W. L. Combined H_2O and CO_2 reforming of CH_4 over nano-sized Ni/$MgO-Al_2O_3$ catalysts for synthesis gas production for gas to liquid (GTL): Effect of Mg/Al mixed ratio on coke formation. *Catal. Today* **2009**, *146*, 166–171.

(27) Jiang, D.; Zhao, B.; Xie, Y.; Pan, G.; Ran, G.; Min, E. Structure and basicity of γ-Al_2O_3-supported MgO and its application to mercaptan oxidation. *Appl. Catal., A* **2001**, *219*, 69–78.

(28) Zhao, B.; Jaing, D.; Xie, Y. Dispersion of Na_2CO_3 on γ-Al_2O_3 and the threshold effect in flue-gas desulfurization. *Fuel* **2002**, *81*, 1565–1568.

(29) Hassanzadeh-Tabrizi, S. A.; Taheri-Nassaj, E. Sol−gel synthesis and characterization of $Al_2O_3-CeO_2$ composite nanopowder. *J. Alloys Compd.* **2010**, *494*, 289–294.

(30) Damyanova, S.; Perez, C. A.; Schmal, M.; Bueno, J. M. C. Characterization of ceria-coated alumina carrier. *Appl. Catal., A* **2002**, *234*, 271–282.

(31) Huang, X.; Huang, H.; Jiang, D.; Zha, B. Investigation of the Structure of γ-Al_2O_3-Supported MgO by Surface Extended Energy Loss Fine Structure. *J. Phys. Chem. A* **2002**, *106*, 2815–281.

(32) Gomez, M. F.; Cadus, L. E.; Abello, M. C. Preparation and characterization of MgO-γ-Al_2 O_3 composite oxides. *Solid State Ionics* **1997**, *98*, 245–249.

(33) Wang, H.; Guan, H.; Duan, L.; Xie, Y. Dispersion of MgO on Pt/c-Al_2O_3 and the threshold effect in NO_x storage. *Catal. Commun.* **2006**, *7*, 802–806.

(34) Xei, Y. C.; Tang, Y. Q. Spontaneous Monolayer Dispersion of Oxides and Salts onto Surfaces of Supports: Applications to Heterogeneous Catalysis. *Adv. Catal.* **1990**, *37*, 1–43.

(35) Vigano, R.; Taraszewska, J.; Daghetti, A.; Trasatti, S. The point of zero charge of RuO_2 + IrO_2 mixed oxides. *J. Electroanal. Chem.* **1985**, *182*, 203–209.